

Theoretical Stability of Ice Shelf Basal Crevasses with a Vertical Temperature Profile

N. B. Coffey^{1,2}, C. Y. Lai^{1,2,3}, Y. Wang³, W. R. Buck⁴, T. Surawy-Stepney⁵,
A. E. Hogg⁵

¹Department of Geophysics, Stanford University, Stanford, CA, USA

²Program in Atmospheric and Oceanic Sciences, Princeton University, Princeton, NJ, USA

³Department of Geosciences, Princeton University, Princeton, NJ, USA

⁴Lamont-Doherty Earth Observatory of Columbia University, New York, NY, USA

⁵School of Earth and Environment, University of Leeds, Leeds, UK

Key Points:

- The effect of vertical temperature structure on the stability of ice shelf basal crevasses varies across several theories.
- Rift formation in each theory depends on dimensionless measures of crack depth, density, ice hardness, and resistive stress.
- Rift formation requires a glaciological stress state near that of a freely-floating ice tongue.

Corresponding author: Niall Coffey, nbc Coffey@stanford.edu

17 **Abstract**

18 Basal crevasses threaten the stability of ice shelves through the potential to form
 19 rifts and calve icebergs. Different existing fracture theories lead to distinct calving pre-
 20 dictions. Furthermore, it is important to determine the dependence of crevasse stabil-
 21 ity on temperature due to large vertical temperature variations on ice shelves. In this
 22 work, we explore the transition from basal crevasses to full thickness fractures consid-
 23 ering the vertical temperature structure. Nye’s Zero-Stress approximation violates New-
 24 ton’s second law. By upholding horizontal force balance, it has been shown analytically
 25 that the threshold stress for rift initiation is that of a freely- floating unconfined ice tongue.
 26 We generalize the force balance argument to show that while temperature structure in-
 27 fluences crack depths, the threshold rifting stress is insensitive to temperature. In the
 28 classical Nye’s theory, basal crevasses would develop into rifts at a stress twice of that
 29 in our Nye’s theory adhering to horizontal force balance.

30 **Plain Language Summary**

31 Ice shelves, the floating extensions of grounded ice sheets, have the ability to slow
 32 down the flow of grounded ice and thus potentially decrease the rate of sea level rise. How-
 33 ever, large fractures can damage ice shelves and reduce their ability to slow down sea
 34 level rise. In this paper, we focus on large fractures on the bottom surface of ice shelves
 35 known as basal crevasses, and under what conditions they break through the full ice thick-
 36 ness to form so-called rifts. We study the role of how a linear temperature profile in the
 37 vertical direction modifies existing fracture theories, with specific focus on what stress
 38 values lead to rifts. We find that including vertical temperature variations can signifi-
 39 cantly alter the transition from basal crevasses to rifts among two existing theories, with
 40 negligible temperature dependence in a recent extension of the simpler theory. Given the
 41 observations of this study, the most accurate theory for predicting rifts has a stress thresh-
 42 old of an unconfined ice tongue, highlighting the sensitivity of ice shelves and importance
 43 of ice shelf buttressing. Future work testing the sensitivities of rift formation stress thresh-
 44 olds will help produce more accurate predictions of ice loss and sea level rise.

45 **1 Introduction**

46 Ice shelf buttressing plays an important role in reducing the rate of sea level rise.
 47 A reduction in buttressing through calving or other processes can increase the mass loss
 48 from ice sheets by increasing the grounding line flux (Thomas & MacAyeal, 1982; Rott
 49 et al., 2002; Rignot et al., 2004; Dupont & Alley, 2005; Pritchard et al., 2012; Haseloff
 50 & Sergienko, 2018). Basal crevasses, vertical fractures on the underside of ice, can play
 51 an important role in the calving process and thus the stability of ice shelves and marine-
 52 terminating glaciers (McGrath, Steffen, Rajaram, et al., 2012; Colgan et al., 2016; Jeong
 53 et al., 2016). Individual basal crevasses can induce surface crevasses, create surface de-
 54 pressions when sufficiently deep that may enable surface meltwater ponding, reduce the
 55 ability of ice shelves to provide back stress to upstream grounded ice, and may penetrate
 56 through the full ice thickness to form rifts (McGrath, Steffen, Scambos, et al., 2012; Luck-
 57 man et al., 2012; Child et al., 2021; Pralong & Funk, 2005). When spaced periodically,
 58 basal crevasses can potentially stabilize ice shelves from breakup through dampening stresses
 59 transmitted through high-frequency elastic-flexural waves (Freed-Brown et al., 2012). The
 60 evolution of basal crevasses has been modeled by the balance of ice shelf and hydrostatic
 61 ocean stresses (Zarrinderakht et al., 2022), as well as idealized ocean dynamics and the
 62 mass balance of melting and freezing (Jordan et al., 2014). Basal crevasses may play a
 63 central role in the flexure-driven calving of marine-terminating glaciers seen in Green-
 64 land and Canada (Wagner et al., 2014; Murray et al., 2015; Wagner et al., 2016; Benn
 65 et al., 2017). In Antarctica, basal crevasses may initiate rifts that can propagate across
 66 the ice shelf and calve icebergs (Lipovsky, 2020). These icebergs can transport fresh melt-

67 water equatorwards and threaten biodiversity of islands in the Southern Ocean (Huth
68 et al., 2022).

69 While the calving of icebergs is likely caused by multiple mechanisms, we focus on
70 the transition from basal crevasses. In the absence of ample surface meltwater such as
71 surface melt ponds, basal crevasses are theoretically more vulnerable than surface crevasses
72 to full-thickness penetration and cause rift initiation (Lai et al., 2020). The depth-averaged
73 deviatoric stress formulations of Nye (Nye, 1955), Weertman (Weertman, 1973), and the
74 zero toughness or half-space formulations of Mode I Linear Elastic Fracture Mechanics
75 (LEFM) (van der Veen, 1998) all predict basal crevasses to be about nine times deeper
76 than dry (water-free) surface crevasses. The magnitude of lithostatic stress only decreases
77 as basal crevasses propagate upwards, yet increases as surface crevasses propagate down-
78 wards, making the initiation of rifts more likely due to basal crevasses than dry surface
79 crevasses. Thus, we study basal crevasses as the precursors of rifts in the absence of strong
80 atmospheric forcing (Morris & Vaughan, 2003; van Wessem et al., 2023).

81 Driven by the importance to predict rift initiation on ice shelves, here we extend
82 analytical and numerical models to predict the ice shelf threshold stress R_{xx} for rifts to
83 initiate from basal crevasses. Our fracture models' deviations from standard implemen-
84 tations and validation of Nye's Zero-Yield Stress (Nye, 1955) and Mode I LEFM for basal
85 crevasses (van der Veen, 1998) are summarized below. First, we include the depth vari-
86 ation of the resistive stress due to vertical temperature variation in all theories and com-
87 pare the results. We chose a linear temperature profile for simplicity and show in Sup-
88 porting Information S5 the effects of a different temperature structure. Second, we mod-
89 ify Nye's Zero-Stress theory to uphold horizontal force balance and include vertical tem-
90 perature variations, following a procedure similar to (Buck, 2023) and obtaining a sim-
91 ple analytical result. Third, we shift the focus from crevasse depth prediction to rift for-
92 mation prediction, analyzing results in terms of stress required for basal crevasses to un-
93 stably propagate and initiate rifts or calving events. Fourth, we validate rift formation
94 predictions with an existing rift catalog (Walker et al., 2013) on the Ross Ice Shelf (RIS)
95 and Larsen C Ice Shelf (LCIS). We verified that the deviation in resistive stress between
96 the 1D fracture theory and the 2D Shallow-Shelf Approximation (SSA) (MacAyeal, 1989)
97 is less than 10%, thus ensuring validity of the 1D flow assumption in the regions of in-
98 terest.

99 **2 Fracture Models of Basal Crevasses with Vertically Varying Ice Tem-** 100 **perature**

101 [Figure 1 about here.]

102 Figure 1 shows the differences between existing isothermal basal crevasse depth predic-
103 tion theories: the Nye's Zero-Stress approximation, LEFM, and a new model based upon
104 Nye's theory in (Buck, 2023). While these theories differ for a range of crack depths, the
105 largest discrepancy is near the sea level, where basal crevasses can unstably propagate
106 and form rifts. Although the basal crevasse to rift transition is challenging to precisely
107 measure (see Supporting Information S2), Figure 1(c-f) motivates our study of rift ini-
108 tiation associated with basal crevasse vertical propagation. Importantly, ice shelves are
109 not isothermal, and basal crevasse depths are sensitive to the ice shelf vertical temper-
110 ature structure (Rist et al., 2002; Borstad et al., 2012; Lai et al., 2020). We analyze sev-
111 eral fracture models (Nye, 1955; van der Veen, 1998; Buck, 2023) and the stress required
112 to form rifts, considering a vertically linear temperature profile for simplicity. We assume
113 that the base of the ice shelf is held at $T_b = -2^\circ\text{C}$, and take a linear temperature pro-
114 file up to the surface temperature T_s as predicted by RACMO (van Wessem et al., 2018).

The Nye's Zero-Stress (Nye, 1955) and LEFM (van der Veen, 1998) theories pre-
sented in this section share many basic assumptions. As shown in Figure 1(a), given a

2D coordinate system with x as the horizontal dimension and z as the vertical dimension, assuming incompressibility and a stress-free upper surface, we can write the net longitudinal stress σ_n of (van der Veen, 1998) at the approximately vertical basal crevasse interface as

$$\sigma_n(z) = R_{xx}(z) - p_l(z) + p_w(z), \quad (1)$$

115 where $R_{xx}(z)$, $p_l(z)$, and $p_w(z)$ are the along-flow component of ice shelf resistive stress
 116 defined in (Cuffey & Paterson, 2010), lithostatic pressure and hydrostatic water pressure,
 117 respectively. We assume that there is negligible vertical shear stress in the ice due
 118 to negligible shear stress on the surface and basal boundaries, thus simplifying the along-
 119 flow component of resistive stress to twice that of the corresponding deviatoric stress com-
 120 ponent, $R_{xx}(z) \approx 2\tau_{xx}(z)$. By setting $z = 0$ at the ice shelf base and positive upwards
 121 as shown in Figure 1(a), we define the pressure terms as $p_l = \rho_i g (H - z)$ and water
 122 pressure $p_w = \rho_w g \max(z_h - z, 0)$, with gravitational acceleration $g = 9.8 \text{ m/s}^2$, verti-
 123 cally integrated ice density $\rho_i = 917 \text{ kg/m}^3$ and ice thickness H . The piezometric head
 124 $z_h = \frac{\rho_i}{\rho_w} H$ as defined in (Nick et al., 2010) depends on the water density; for this study,
 125 we assume constant saltwater density $\rho_w = 1028 \text{ kg/m}^3$.

The way that we account for vertical temperature structure $T(z)$ is through the ice hardness $B(T)$ in the effective viscosity. Modeling ice as a Non-Newtonian power-law fluid (Glen, 1958), the effective viscosity is,

$$\mu = \frac{B(T)}{2} \dot{\epsilon}_e^{\frac{1}{n}-1} \approx \frac{B(T)}{2} \dot{\epsilon}_{xx}^{\frac{1}{n}-1}, \quad (2)$$

where the effective strain rate $\dot{\epsilon}_e$, i.e. the second invariant of the strain rate tensor $\dot{\epsilon}_{ij}$, is dominated by the along-flow component $\dot{\epsilon}_{xx}$. Thus, the along-flow resistive stress $R_{xx} = 2\tau_{xx} = 4\mu\dot{\epsilon}_{xx}$ can be written as

$$R_{xx} = 2B(T) \dot{\epsilon}_{xx}^{\frac{1}{n}}. \quad (3)$$

Based on lab experiments, the Glen's flow law gives $n = 3$ (Glen, 1958), and $B(T)$ (LeB. Hooke, 1981) can be expressed as

$$B(T) = B_0 \exp \left[\frac{T_0}{T} - \frac{C}{(T_r - T)^k} \right], \quad (4)$$

126 where $B_0 = 2.207 \text{ Pa} \cdot \text{yr}^{\frac{1}{n}}$, $T_0 = 3155 \text{ K}$, $T_r = 273.39 \text{ K}$, $k = 1.17$, and $C = 0.16612$
 127 K^k are constants determined from empirical fit (LeB. Hooke, 1981).

128 2.1 Nye's Zero-Yield Stress

Nye's theory (Nye, 1955) assumes that a crevasse will propagate until infinitesimal crack tip growth would put the net longitudinal stress σ_n at the crack tip into compression. Nye's theory is self-consistent when surface and basal crevasses are both allowed to propagate. As derived in Supporting Information S3, a basal crevasse on a freely-floating ice shelf can unstably propagate to the surface when the resistive stress is above the threshold

$$\frac{\overline{R_{xx}}}{\overline{R_{xx}}^{IT}} \geq 2 \frac{\rho_w}{\rho_i} \frac{d_b^*}{H} \frac{\overline{\tilde{B}(T)}}{\tilde{B}\left(T\left(\frac{d_b^*}{H}\right)\right)}. \quad (5)$$

129 In this equation, the overline \bar{q} represents a depth-averaged value for the variable q . The
 130 dimensionless numbers involved are the depth-averaged resistive stress $\overline{R_{xx}}$ relative to
 131 the isothermal ice tongue resistive stress $\overline{R_{xx}}^{IT} \equiv \frac{1}{2} \left(1 - \frac{\rho_i}{\rho_w}\right) \rho_i g H$ as derived by (Weertman,
 132 1957); the ratio of densities ρ_w/ρ_i ; the unstable basal crevasse depth relative to ice thick-
 133 ness d_b^*/H ; the nondimensional ice hardness $\tilde{B}(T) \equiv \frac{B(T)}{B(T(z=0))}$; and the nondimensional
 134 ice hardness at the unstable basal crevasse depth $\tilde{B}\left(T\left(\frac{d_b^*}{H}\right)\right)$. Note that when we treat

135 the ice as isothermal, the ice hardness ratio $\overline{\tilde{B}(T)}/\tilde{B}\left(T\left(\frac{d_b^*}{H}\right)\right)$ is 1, and the maximum
 136 basal crevasse depth is from the base to sea level $\frac{\rho_w}{\rho_i}\frac{d_b^*}{H} = 1$, making the right-hand side
 137 of equation (5) 2. Thus, under Nye’s Zero-Stress theory, a basal crevasse will propagate
 138 to the sea level, intersecting a surface crevasse to form a rift in isothermal ice when the
 139 depth-averaged resistive stress is twice that of an isothermal ice tongue, as shown in Fig-
 140 ure 1(b).

141 The simplicity of Nye’s theory comes with limitations. Nye’s original theory does
 142 not include stress concentration near crack tips, the material strength of ice, accumu-
 143 lation and melt, nor crevasse-induced stresses. The lack of stress concentration and zero
 144 material strength is applicable in the limit of closely-spaced crevasses (De Robin, 1974;
 145 Weertman, 1974), where the spacing between crevasses is much less than the individual
 146 crevasse depths (Weertman, 1977). Observations indicate basal crevasse spacing to be
 147 roughly one to several ice thicknesses (Luckman et al., 2012; McGrath, Steffen, Rajaram,
 148 et al., 2012; Lawrence et al., 2023), breaking the densely-spaced crevasses assumption
 149 in Nye’s theory. Recent extensions of Nye’s theory include non-zero material strength
 150 (Benn et al., 2007) and accumulation and melting effects (Bassis & Ma, 2015; Huth et
 151 al., 2021). In the limit of densely-spaced crevasses with negligible flexural stress, the ef-
 152 fects of crevasse-induced stress on crack depth has been included to satisfy a horizon-
 153 tal force balance argument (Buck, 2023). We present an approach to generalize this ap-
 154 proximate crevasse-induced stress for vertically varying ice temperature in Section 2.3.

155 2.2 Linear Elastic Fracture Mechanics

156 In contrast to the Nye’s theory, the Linear Elastic Fracture Mechanics (LEFM) frame-
 157 work applied by (van der Veen, 1998) considers an isolated basal crevasse with stress con-
 158 centration near the crack tip. LEFM agrees with the analytical approach of including
 159 stress concentration near crack tips by Weertman (Weertman, 1973) for small crack depths
 160 (Buck & Lai, 2021). Unlike Weertman’s infinite thickness assumption (Weertman, 1973),
 161 LEFM comes with the advantage of accounting for a prescribed finite thickness (van der
 162 Veen, 1998), making it well suited for determining rift initiation stresses. The LEFM rift-
 163 ing threshold $\overline{R_{xx}^*}$ for an isothermal ice shelf with traction-free upper and lower surfaces
 164 had been reported by (Zarrinderakht et al., 2022) and (Lai et al., 2020). Building on the
 165 work of (van der Veen, 1998; Tada et al., 2000; Lai et al., 2020), we extended the LEFM
 166 analysis across a range of surface temperatures applicable to Antarctica and present the
 167 rifting threshold $\overline{R_{xx}^*}$ for a vertically varying ice temperature. One of the largest sim-
 168 plifications of this version of LEFM is having stress-free upper and lower surface bound-
 169 ary conditions, thus neglecting the oceanic restoring force associated with the vertical
 170 displacement at the ice-ocean boundary (Jiménez & Duddu, 2018; Huth et al., 2021; Zarrinder-
 171 akht et al., 2022). Future work is needed to account for the oceanic restoring force.

172 2.3 Nye’s Zero-Yield Stress with Horizontal Force Balance

173 Here, we parameterize the crevasse-induced compressive stress through Nye’s frame-
 174 work and an Eulerian control volume approach to describe vertically-varying tempera-
 175 ture profiles. Note that the control volume argument is Newton’s Second Law, and our
 176 assumptions of glaciostatic balance and stress distribution represent the limiting case of
 177 a densely-crevassed ice shelf where flexural stresses are negligible. In order to satisfy hor-
 178 izontal force balance (HFB), the extra compressive stresses in the unbroken ligament be-
 179 tween the surface and basal crevasse tips, induced by the crevasses themselves, needs to
 180 be considered. As in Supporting Information S4, we parameterize this crevasse-induced
 181 stress to uphold the zero material strength assumption of Nye’s theory, continuity of stress
 182 at crack tips (Buck & Lai, 2021), and horizontal force balance (Buck, 2023).

Our fixed control volume has vertical boundaries at the ice shelf surface and base, and horizontal boundaries at the symmetry plane of a basal crevasse, $x = x_c$, and at a nearby downstream location $x = x_c + \Delta x$ with the same ice thickness and temperature profile, as depicted in Figure 1. Taking glaciostatic balance (Lindstrom & MacAyeal, 1987),

$$\partial_z \sigma_{zz} = \rho_i g, \quad (6)$$

we can integrate from a level z to the surface H and solve for pressure as $p \equiv -\sigma_{zz} + \tau_{zz} = \rho_i g (H - z) + \tau_{zz}$ using a stress-free upper surface boundary condition. From the downstream side of the control volume at $x = x_c + \Delta x$, the ice shelf Cauchy stress can be written as

$$\sigma_{xx}(x_c + \Delta x, z) \equiv -p + \tau_{xx} = -\rho_i g (H - z) - \tau_{zz} + \tau_{xx} = -\rho_i g (H - z) + R_{xx}(z), \quad (7)$$

183 where 2D incompressibility gives $\tau_{xx} = -\tau_{zz}$. Note that this stress distribution is valid
184 for an uncrevassed location, where there is no basal crevasse-induced flexural stress.

At $x = x_c$ the stress can be written in a piecewise fashion corresponding to a dry surface crevasse of depth d_s ($H - d_s \leq z \leq H$), a water-filled basal crevasse of depth d_b ($0 \leq z \leq d_b$), and a solid ice ligament between the two ($d_b \leq z \leq H - d_s$),

$$\sigma_{xx}(x_c, z) = \begin{cases} 0, & H - d_s \leq z \leq H \quad (\text{surface crevasse}) \\ -\rho_i g (H - z) + c R_{xx}(z), & d_b \leq z \leq H - d_s \quad (\text{unbroken ice}) \\ -\rho_w g (z_h - z), & 0 \leq z \leq d_b \quad (\text{basal crevasse}) \end{cases} \quad (8)$$

185 Here, $c R_{xx}(z)$ represents the sum of the background resistive stress and the crevasse-induced
186 compressive stress in the unbroken ice ligament. We use a constant multiplier c to up-
187 hold the zero strength assumption and enforce horizontal force balance, as adding a con-
188 stant will impose a non-zero material strength. Investigations of material strength ef-
189 fects and crevasse-induced flexural stresses are subject to future work.

When the crack is stable, the crevasse depth is instantaneously determined by the stress states. This is consistent with Nye's and (van der Veen, 1998)'s basal crevasse LEFM consideration neglecting time-dependent fracture propagation, but is a possible future extension (Lawn, 1993). Due to the horizontal force balance on an Eulerian or fixed control volume, defined with negligible inertial term as

$$0 = \int_0^H \int_{x_c}^{x_c + \Delta x} [\partial_x \sigma_{xx} + \partial_z \tau_{zx}] dx dz, \quad (9)$$

the negligible shear stress on the upper and lower surfaces simplifies equation (9) such that the sum of the horizontal forces per unit width into the page on our control volume is zero,

$$\int_0^H [\sigma_{xx}(x_c + \Delta x) - \sigma_{xx}(x_c)] dz = 0. \quad (10)$$

Solving for the constant c and finding a relation between surface and basal crack depths will close the system of equations, allowing us to determine crevasse depths given a normalized resistive stress $\bar{R}_{xx}/\bar{R}_{xx}^{IT}$. Following (Buck & Lai, 2021), we use continuity of stress at crack tips, $z = H - d_s$ and $z = d_b$, as a constraint to determine the constant c and then a relation between the crevasse depths. At the tip of the surface crevasse, we have that

$$0 = -\rho_i g d_s + c(R_{xx})|_{z=H-d_s}, \quad (11)$$

which easily resolves the constant as

$$c = \frac{\rho_i g d_s}{(R_{xx})|_{z=H-d_s}}. \quad (12)$$

At the basal crevasse tip, we have that

$$-\rho_i g H + \rho_w g d_b = -\rho_i g (H - d_b) + \frac{\rho_i g d_s}{(R_{xx})|_{z=H-d_s}} (R_{xx})|_{z=d_b}, \quad (13)$$

which can readily be simplified to a dimensionless relation between basal and surface crack depth,

$$\frac{d_b}{d_s} = \frac{\rho_i}{\rho_w - \rho_i} \frac{B(T|_{z=d_b})}{B(T|_{z=H-d_s})}. \quad (14)$$

190 Thus the temperature profile $T(z)$ affects the relative surface to basal crevasse depth through
191 $B(T(z))$, with colder surface temperatures creating larger crevasse depth ratio d_s/d_b .

Having solved for the constant, we may now evaluate the force balance constraint of equation (10) with the stress expressions in equations (7) and (8). Defining the dimensionless variables $\tilde{d}_b = d_b/H$, $\tilde{d}_s = d_s/H$, and $\tilde{z} = z/H$, the dimensionless force balance can be written as

$$\frac{\bar{R}_{xx}}{\bar{R}_{xx}^{IT}} = \frac{\rho_w}{\rho_w - \rho_i} \tilde{d}_s^2 + \frac{\rho_w}{\rho_i} \tilde{d}_b^2 + \frac{\tilde{d}_s}{\frac{1}{2} \left(1 - \frac{\rho_i}{\rho_w}\right)} \int_{\tilde{d}_b}^{1-\tilde{d}_s} \tilde{B}(T(\tilde{z})) d\tilde{z}. \quad (15)$$

192 Equations (14) and (15) form a system of two equations with the surface and basal crack
193 depths as the two unknowns, given that $\bar{R}_{xx}/\bar{R}_{xx}^{IT}$ is known. For isothermal ice shelves,
194 ice hardness functions become constants as in equation (S12), and the equation has an
195 analytical solution as presented in equation (S17) (Buck, 2023).

196 When we include the vertical temperature structure, we compute the ice hardness
197 function given vertical temperature variation numerically. We iterate through temper-
198 ature profiles and basal crevasse depths to solve for surface crevasse depth through the
199 equation residual of equation (14). Having numerically obtained a relation between \tilde{d}_b
200 and \tilde{d}_s , we use these values to solve for $\bar{R}_{xx}/\bar{R}_{xx}^{IT}$ in equation (15). We plot dimension-
201 less basal crack depth as a function of $\bar{R}_{xx}/\bar{R}_{xx}^{IT}$ for the linear vertical temperature case
202 in Figure 2. Importantly, we find that the crevasse to rift transition for cold and warm
203 ice shelf surface temperatures occurs at roughly the same critical stress. Thus, Nye's the-
204 ory with Horizontal Force Balance can be approximated by a simple analytical rifting
205 criteria that is independent of the vertical temperature structure,

$$\frac{\bar{R}_{xx}^*}{\bar{R}_{xx}^{IT}} = 1. \quad (16)$$

206 2.4 Comparison between the three fracture models

207 The comparison between the three fracture models is presented in Figure 2. In or-
208 der of smallest to largest rifting threshold $\bar{R}_{xx}^*/\bar{R}_{xx}^{IT}$, or highest to lowest vulnerability
209 to rifting, we have LEFM, Nye's with Horizontal Force Balance (HFB), and Nye's orig-
210 inal theory for all temperatures analyzed in this study. We note that the influence of tem-
211 perature is distinct between the three theories; while Nye's with HFB has negligible tem-
212 perature dependence, colder surface temperatures lower the rifting threshold $\bar{R}_{xx}^*/\bar{R}_{xx}^{IT}$
213 for Nye's original theory yet increase the rifting threshold for LEFM. However, for Nye's
214 with Horizontal Force Balance in Figure 2b), colder surface temperatures cause a decrease
215 (increase) in basal (surface) crevasse depth, yet leave the rifting threshold stress unchanged.
216 Thus, the effect of temperature on basal crevasse depth and rift initiation depends strongly
217 on the chosen theory.

218 [Figure 2 about here.]

219 3 Comparison with Observations

220 [Figure 3 about here.]

221 As the three fracture theories predict distinct critical stresses that drive the basal
 222 crevasse to rift transition, we evaluate the applicability of each theory by comparison with
 223 observed rift locations. We analyze our results in two ways. First, we plot the predicted
 224 rift locations on MODIS MOA (Scambos et al., 2007; Haran et al., 2018) compared with
 225 the rifts previously mapped by (Walker et al., 2013) (labeled as “true rifts”) on Ross Ice
 226 Shelf (RIS) in Figure 3. The goal of these rift formation theories is to maximize the over-
 227 lap between the predicted and true rifts, colored in green in Figure 3. Because we do not
 228 have values of strain rate or surface temperature at the time of rifting, the estimated stress
 229 state uses modern surface temperature (van Wessem et al., 2018) and strain rate (Wearing,
 230 2017) values, with limitations discussed in Supporting Information S1. In Figure 3, we
 231 see that on the RIS rifts identified by (Walker et al., 2013), Nye’s theory with vertical
 232 temperature structure underpredicts known rifts as shaded in blue. Similarly, LEFM with
 233 a depth-averaged resistive stress, with analytical result given by (Zarrinderakht et al.,
 234 2022), overpredicts rifts into areas they were not observed as shaded in red. However,
 235 LEFM with vertical temperature structure and Nye’s theory with Horizontal Force Bal-
 236 ance are the most accurate theories for these RIS rifts. Their differences are small enough
 237 to warrant more observations to distinguish which theory is most applicable.

238 [Figure 4 about here.]

239 Second, we construct a crack stability plot of the critical stress $\bar{R}_{xx}^*/\bar{R}_{xx}^{IT}$ for rift
 240 formation for each theory as a function of the ice surface temperature T_s , as shown by
 241 the curves in Figure 4. Noticeably, surface temperature has a negligible effect on the rift-
 242 ing threshold for the Nye’s theory with Horizontal Force Balance; the rifting stress is that
 243 of a freely-floating ice tongue, $\bar{R}_{xx}^* = \bar{R}_{xx}^{IT} \equiv \frac{1}{2} \left(1 - \frac{\rho_i}{\rho_w}\right) \rho_i g H$. Comparing the rift for-
 244 mation stress criteria, the depth-averaged Nye’s theory requires a resistive stress 200%
 245 that of a freely-floating ice tongue to cause rifts, while the depth-averaged formulation
 246 for LEFM as presented by (Zarrinderakht et al., 2022) requires only 74% of that of a freely-
 247 floating ice tongue to initiate rifts. It is our goal to constrain this substantial uncertainty
 248 in the rift initiation stress threshold of these two classical theories, presented by the dashed
 249 lines of Figure 4.

250 We quantitatively compare the rift criteria with the observed rifts on the RIS in
 251 Figure 3 and Larsen C Ice Shelf (LCIS) in Figure S3. We identify the extensional, 1D
 252 flow regions excluding the rift locations on the RIS and LCIS in Figure S4, and plot the
 253 mean depth-averaged resistive stress and surface temperature across these regions in or-
 254 ange on Figure 4 with one standard deviation of uncertainty due to the variation of re-
 255 sistive stress and surface temperature across these regions. The bulk of the non-rift ice
 256 shelf data should lie below the curves in Figure 4. While LEFM with depth-averaged re-
 257 sistive stress may look accurate on Figure 4, the overprediction in red is clear in Figures
 258 3c) and S3c). Additionally, the lack of force balance from classical Nye (1955)’s (dashed
 259 blue line) and classical Nye (1955)’s with vertical temperature variation (solid green line)
 260 invalidates these predictions on theoretical grounds. This lack of force balance manifests
 261 as an underprediction of rifting, as discussed in Supporting Information S1 and demon-
 262 strated in Figure S9. Therefore, within the uncertainty of our data as discussed in Sup-
 263 porting Information S5, our results on two ice shelves suggest LEFM and Nye’s with Hor-
 264 izontal Force Balance considering the vertically varying ice temperatures are the most
 265 accurate theories for classifying the RIS and LCIS ice shelf data as containing or not con-
 266 taining a rift.

267 4 Discussion and Conclusions

268 In this paper, we have determined several rift formation stress criteria as functions
 269 of surface temperature for linear temperature profiles. We then use remote-sensing and
 270 model output data to determine which theory best predicts observed rifts. We find that

271 Nye’s Zero-Stress with either depth-averaged or vertically-varying resistive stress under-
 272 predicts rifts, due in part to the inconsistency that the formulations do not uphold force
 273 balance as first argued in (Buck, 2023). On the other hand, we find that LEFM with depth-
 274 averaged resistive stress overpredicts rifts. Our result shows that on the RIS and LCIS
 275 ice shelves, Nye’s theory with Horizontal Force Balance and LEFM with vertically-varying
 276 resistive stress are the most accurate theories for correctly predicting rifts and non-rifts.
 277 Further distinction between these two theories is inhibited by the number of rifts and
 278 uncertainty of current data products used in this study. However, given that buoyancy
 279 is expected to stabilize basal crevasses (Zarrinderakht et al., 2022) and is not available
 280 analytically for the LEFM models, we expect the rift initiation stress threshold of LEFM
 281 models to increase. Thus, we recommend the simple, analytical, temperature-independent
 282 formulation of Nye’s with HFB’s rift initiation threshold $\bar{R}_{xx}^*/\bar{R}_{xx}^{IT} = 1$ of equation (16),
 283 which is both self-consistent and validated against observed rifts on RIS and LCIS. We
 284 find a negligible temperature dependence of this rifting threshold. This result appears
 285 robust to the choice of temperature profile, having been confirmed in Supporting Infor-
 286 mation S5 for a Robin temperature profile (Robin, 1955).

287 A question may then naturally arise: How can the freely-floating ice tongue stress
 288 be sufficient to form rifts, yet we see ice tongues exist in nature? It is important here
 289 to draw a distinction between idealized ice tongues and those found in nature: any per-
 290 turbations to the stress field will influence the stability of real ice tongues. For exam-
 291 ple, sea ice or ice mélange can stabilize these structures through potentially providing
 292 a force buttressing the ice shelf and dampening ocean waves that would otherwise in-
 293 duce ice shelf flexural stress (Vaughan, 1995; Bromirski et al., 2010; Sergienko, 2010, 2013;
 294 Hulbe et al., 2016; Massom et al., 2018; Gomez-Fell et al., 2022). Indeed, recent obser-
 295 vational work analyzing the eastern Antarctic Peninsula found that 94% of calving oc-
 296 curred during or shortly after the removal of sea ice (Christie et al., 2022).

297 This idealized study is subject to several limitations. We assume 2D (x, z) , incom-
 298 pressible, homogeneous density, elastic modulus, and fracture toughness (Rist et al., 2002)
 299 ice shelves with zero across-flow strain rate and zero shear strain rate. These theories
 300 do not include local thickness variation, creep closure, sub- and super-buoyant flexure
 301 (Benn et al., 2017), ice front bending stresses (Reeh, 1968), grain size dependence of yield
 302 stress (Ranganathan et al., 2021), snow accumulation, basal melting (Bassis & Ma, 2015;
 303 Buck, 2023), and marine ice accumulation. In taking a constant density, we argue with
 304 (van der Veen, 1998; Lai et al., 2020) that variations due to firn and an equation of state
 305 for ice (Feistel & Wagner, 2006) are negligible for basal crevasse propagation. To uphold
 306 the plane strain assumptions of our fracture theories when comparing with observations,
 307 we develop a strain rate criteria in Supporting Information S1 to validate locations where
 308 the flow is approximately 1D and Mode I fracture is applicable. In reality, ice shelves
 309 can also have their stress states altered due to 3D effects such as shear fractures (van der
 310 Veen, 1999) and torque from ocean currents (Gomez-Fell et al., 2022; Huth et al., 2022).
 311 The interactions of the ocean, sea ice, mass balance, or other additional stresses may de-
 312 termine the stability of the ice tongues and shelves in nature by modulating the ice shelf
 313 stress. Effects such as the hydrographic environment in basal crevasses, crevasse-, tidal-
 314 , or tsunami-induced flexural stresses (Walker et al., 2013; Brunt et al., 2011; Bromirski
 315 et al., 2017; Gerstoft et al., 2017), viscous creep closure, realistic ice rheology, or the time-
 316 dependent evolution of basal crevasses evolving into rifts are neglected. We leave the cou-
 317 pling of these processes to future work.

318 With higher temporal-resolution strain rate estimates than presented in Figure 1(c),
 319 cross-rift altimetry, and/or field-based data of the basal crevasse to rift transition, these
 320 rifting stress threshold theories provide a basis for comparison. This study provides a
 321 simple analytical rift formation stress threshold that can be coupled with numerical ice-
 322 sheet simulations. One application could be to enforce that the vertical principal com-
 323 ponent of damage becomes one from (Huth et al., 2021) when the stress state is above

324 the rift formation stress threshold. In terms of theory, this study advances the common
 325 fracture theories used in glaciology through the incorporation of vertical stress variations
 326 due to the temperature dependence of the ice hardness, and the modifications of Nye's
 327 theory to properly account for horizontal force balance. An interesting extension would
 328 be applying Nye's with HFB to the analysis of the ice shelf necking instability developed
 329 by (Bassis & Ma, 2015). The different rifting stress theories coupled with ice shelf sim-
 330 ulations can lead to distinct calving predictions. Importantly, the classical Nye's theory
 331 would largely under-predict the ice mass loss compared with the Nye's with HFB, and
 332 impact the sea level projection over the coming centuries.

333 Data Availability Statement

334 Strain rates are calculated with the Antarctic velocity field from MEaSUREs Phase-
 335 Based Antarctica Ice Velocity Map, Version 1 (NSIDC-0754), available at <https://nsidc.org/data/nsidc-0754/versions/1>. The Antarctic ice thickness field is from MEaSUREs
 336 BedMachine Antarctica, Version 2 (NSIDC-0756), available at <https://nsidc.org/data/nsidc-0756/versions/2>. The RACMO 2.3p2 Antarctic surface temperature data are
 337 available from <https://doi.org/10.5281/zenodo.7845736>. The MEaSUREs MODIS
 338 Mosaic of Antarctica 2013-2014 (MOA2014) Image Map, Version 1 is available at <https://nsidc.org/data/NSIDC-0730/versions/1>. The ENVEO monthly Antarctic velocity
 339 data are available at <https://dx.doi.org/10.5285/00fe090efc58446e8980992a617f632f>.

343 Author Contribution

344 N.B.C. and C.-Y.L. conceived the study. N.B.C. led the project, numerical and data
 345 analysis, and the preparation of the manuscript. Y.W. and W.R.B. contributed to the
 346 model discussions. T.S. and A.E.H. processed the strain rates estimates and SAR im-
 347 ages in Figure 1, and wrote the corresponding supplementary section on temporal ob-
 348 servation.

349 Acknowledgments

350 We acknowledge funding from NSF's Office of Polar Programs through OPP-2235051.

351 References

- 352 Bassis, J., & Ma, Y. (2015). Evolution of basal crevasses links ice shelf stability
 353 to ocean forcing. *Earth and Planetary Science Letters*, *409*, 203-211. Re-
 354 trieved from <https://www.sciencedirect.com/science/article/pii/S0012821X14006840> doi: <https://doi.org/10.1016/j.epsl.2014.11.003>
- 355 Benn, D. I., Hulton, N. R. J., & Mottram, R. H. (2007). 'Calving laws', 'sliding
 356 laws' and the stability of tidewater glaciers. *Annals of Glaciology*, *46*, 123-130.
 357 Retrieved 2023-04-17, from <https://www.cambridge.org/core/journals/annals-of-glaciology/article/calving-laws-sliding-laws-and-the-stability-of-tidewater-glaciers/2B0D6FD7FBEBAB83BA1F4522F37C5CBF>
 358 (Publisher: Cambridge University Press) doi: 10.3189/172756407782871161
- 359 Benn, D. I., Åström, J., Zwinger, T., Todd, J., Nick, F. M., Cook, S., ... Luckman,
 360 A. (2017). Melt-under-cutting and buoyancy-driven calving from tidewater
 361 glaciers: new insights from discrete element and continuum model simulations.
 362 *Journal of Glaciology*, *63*(240), 691-702. doi: 10.1017/jog.2017.41
- 363 Borstad, C. P., Khazendar, A., Larour, E., Morlighem, M., Rignot, E., Schod-
 364 lok, M. P., & Seroussi, H. (2012). A damage mechanics assessment of
 365 the larsen b ice shelf prior to collapse: Toward a physically-based calv-
 366 ing law. *Geophysical Research Letters*, *39*(18). Retrieved from <https://>

- 370 [agupubs.onlinelibrary.wiley.com/doi/abs/10.1029/2012GL053317](https://doi.org/10.1029/2012GL053317) doi:
371 <https://doi.org/10.1029/2012GL053317>
- 372 Bromirski, P. D., Chen, Z., Stephen, R. A., Gerstoft, P., Arcas, D., Diez, A., ...
373 Nyblade, A. (2017). Tsunami and infragravity waves impacting antarctic
374 ice shelves. *Journal of Geophysical Research: Oceans*, *122*(7), 5786-5801.
375 Retrieved from [https://agupubs.onlinelibrary.wiley.com/doi/abs/](https://agupubs.onlinelibrary.wiley.com/doi/abs/10.1002/2017JC012913)
376 [10.1002/2017JC012913](https://doi.org/10.1002/2017JC012913) doi: <https://doi.org/10.1002/2017JC012913>
- 377 Bromirski, P. D., Sergienko, O. V., & MacAyeal, D. R. (2010). Transoceanic
378 infragravity waves impacting Antarctic ice shelves. *Geophysical*
379 *Research Letters*, *37*(2). Retrieved 2023-02-27, from [https://](https://onlinelibrary.wiley.com/doi/abs/10.1029/2009GL041488)
380 onlinelibrary.wiley.com/doi/abs/10.1029/2009GL041488 (eprint:
381 <https://onlinelibrary.wiley.com/doi/pdf/10.1029/2009GL041488>) doi:
382 [10.1029/2009GL041488](https://doi.org/10.1029/2009GL041488)
- 383 Brunt, K. M., Okal, E. A., & MacAyeal, D. R. (2011). Antarctic ice-shelf calving
384 triggered by the honshu (japan) earthquake and tsunami, march 2011. *Journal*
385 *of Glaciology*, *57*(205), 785-788. doi: [10.3189/002214311798043681](https://doi.org/10.3189/002214311798043681)
- 386 Buck, W. R. (2023). The role of fresh water in driving ice shelf crevassing, rift-
387 ing and calving. *Earth and Planetary Science Letters*, *624*, 118444. Re-
388 trieved from [https://www.sciencedirect.com/science/article/pii/](https://www.sciencedirect.com/science/article/pii/S0012821X23004570)
389 [S0012821X23004570](https://doi.org/10.1016/j.epsl.2023.118444) doi: <https://doi.org/10.1016/j.epsl.2023.118444>
- 390 Buck, W. R., & Lai, C.-Y. (2021). Flexural control of basal crevasse opening under
391 ice shelves. *Geophysical Research Letters*, *48*(8), e2021GL093110. Retrieved
392 from [https://agupubs.onlinelibrary.wiley.com/doi/abs/10.1029/](https://agupubs.onlinelibrary.wiley.com/doi/abs/10.1029/2021GL093110)
393 [2021GL093110](https://doi.org/10.1029/2021GL093110) (e2021GL093110 2021GL093110) doi: [https://doi.org/10.1029/](https://doi.org/10.1029/2021GL093110)
394 [2021GL093110](https://doi.org/10.1029/2021GL093110)
- 395 Child, S. F., Stearns, L. A., van der Veen, C. J., & Elósegui, P. (2021). Basal
396 crevasse formation on byrd glacier, east antarctica, as proxy for past sub-
397 glacial flooding events. *Geophysical Research Letters*, *48*(15), e2020GL090978.
398 Retrieved from [https://agupubs.onlinelibrary.wiley.com/doi/abs/](https://agupubs.onlinelibrary.wiley.com/doi/abs/10.1029/2020GL090978)
399 [10.1029/2020GL090978](https://doi.org/10.1029/2020GL090978) (e2020GL090978 2020GL090978) doi: [https://](https://doi.org/10.1029/2020GL090978)
400 doi.org/10.1029/2020GL090978
- 401 Christie, F. D., Benham, T. J., Batchelor, C. L., Rack, W., Montelli, A., &
402 Dowdeswell, J. A. (2022). Antarctic ice-shelf advance driven by anomalous
403 atmospheric and sea-ice circulation. *Nature Geoscience*, *15*(5), 356-362.
- 404 Colgan, W., Rajaram, H., Abdalati, W., McCutchan, C., Mottram, R., Moussavi,
405 M. S., & Grigsby, S. (2016). Glacier crevasses: Observations, models, and mass
406 balance implications. *Reviews of Geophysics*, *54*(1), 119-161. Retrieved
407 from [https://agupubs.onlinelibrary.wiley.com/doi/abs/10.1002/](https://agupubs.onlinelibrary.wiley.com/doi/abs/10.1002/2015RG000504)
408 [2015RG000504](https://doi.org/10.1002/2015RG000504) doi: <https://doi.org/10.1002/2015RG000504>
- 409 Cuffey, K. M., & Paterson, W. S. B. (2010). *The physics of glaciers*. Academic
410 Press.
- 411 De Robin, G. Q. (1974). Depth of water-filled crevasses that are closely spaced.
412 *Journal of Glaciology*, *13*(69), 543-543. doi: [10.3189/S002214300023285](https://doi.org/10.3189/S002214300023285)
- 413 Dupont, T. K., & Alley, R. B. (2005). Assessment of the importance of ice-shelf but-
414 tressing to ice-sheet flow. *Geophysical Research Letters*, *32*(4). Retrieved
415 from [https://agupubs.onlinelibrary.wiley.com/doi/abs/10.1029/](https://agupubs.onlinelibrary.wiley.com/doi/abs/10.1029/2004GL022024)
416 [2004GL022024](https://doi.org/10.1029/2004GL022024) doi: <https://doi.org/10.1029/2004GL022024>
- 417 Feistel, R., & Wagner, W. (2006). A new equation of state for h₂o ice ih. *Journal*
418 *of Physical and Chemical Reference Data*, *35*(2), 1021-1047. Retrieved from
419 <https://doi.org/10.1063/1.2183324> doi: [10.1063/1.2183324](https://doi.org/10.1063/1.2183324)
- 420 Freed-Brown, J., Amundson, J. M., MacAyeal, D. R., & Zhang, W. W. (2012).
421 Blocking a wave: frequency band gaps in ice shelves with periodic crevasses.
422 *Annals of Glaciology*, *53*(60), 85-89. Retrieved 2023-02-27, from [https://](https://www.cambridge.org/core/journals/annals-of-glaciology/article/blocking-a-wave-frequency-band-gaps-in-ice-shelves-with-periodic)
423 [www.cambridge.org/core/journals/annals-of-glaciology/article/](https://www.cambridge.org/core/journals/annals-of-glaciology/article/blocking-a-wave-frequency-band-gaps-in-ice-shelves-with-periodic)
424 [blocking-a-wave-frequency-band-gaps-in-ice-shelves-with-periodic](https://doi.org/10.1017/S0022214312000000)

425 -crevasses/3301ACE8900CFE5D18B2CBC9F1B3B5D1 (Publisher: Cambridge
 426 University Press) doi: 10.3189/2012AoG60A120

427 Gerstoft, P., Bromirski, P., Chen, Z., Stephen, R. A., Aster, R. C., Wiens, D. A., & Nyblade,
 428 A. (2017, 05). Tsunami excitation of the Ross Ice Shelf, Antarctica. *The Journal of*
 429 *the Acoustical Society of America*, 141(5supplement), 3526 – 3526. Retrieved from doi:
 430 10.1121/1.4987434

431 Glen, J. (1958). The flow law of ice: A discussion of the assumptions made in glacier
 432 theory, their experimental foundations and consequences. *IASH Publ*, 47(171), e183.
 433

434 Gomez-Fell, R., Rack, W., Purdie, H., & Marsh, O. (2022). Parker ice tongue collapse,
 435 antarctica, triggered by loss of stabilizing land-fast sea ice. *Geophysical Research Let-*
 436 *ters*, 49(1), e2021GL096156. Retrieved from [https://agupubs.onlinelibrary.wiley](https://agupubs.onlinelibrary.wiley.com/doi/abs/10.1029/2021GL096156)
 437 [.com/doi/abs/10.1029/2021GL096156](https://agupubs.onlinelibrary.wiley.com/doi/abs/10.1029/2021GL096156) (e2021GL096156 2021GL096156) doi: [https://](https://doi.org/10.1029/2021GL096156)
 438 doi.org/10.1029/2021GL096156

439 Haran, T., Bohlander, J., Scambos, T., Painter, T., & Fahnestock, M. (2013). 2005,
 440 updated 2013. modis mosaic of antarctica 2003-2004 (moa2004) image map, version 1.
 441 moa125_r1_hp1.img.gz. (Boulder, Colorado USA. NASA National Snow and Ice Data
 442 Center Distributed Active Archive Center. doi: <http://dx.doi.org/10.7265/N5ZK5DM5>.
 443 Accessed 14/06/2021.)

444 Haran, T., Klinger, M., Bohlander, J., Fahnestock, M., Painter, T., & Scambos., T. (2018).
 445 Measures modis mosaic of antarctica 2013-2014 (moa2014) image map, version 1. NASA
 446 National Snow and Ice Data Center Distributed Active Archive Center. Retrieved from
 447 <https://nsidc.org/data/NSIDC-0730/versions/1> doi: 10.5067/RNF17BP824UM
 448

449 Haseloff, M., & Sergienko, O. V. (2018). The effect of buttressing on grounding line
 450 dynamics. *Journal of Glaciology*, 64(245), 417–431. doi: 10.1017/jog.2018.30

451 Hulbe, C. L., Klinger, M., Masterson, M., Catania, G., Cruikshank, K., & Bugni, A. (2016,
 452 October). Tidal bending and strand cracks at the Kamb Ice Stream grounding line, West
 453 Antarctica. *Journal of Glaciology*, 62(235), 816–824. Retrieved 2023-01-30, from [https://](https://www.cambridge.org/core/journals/journal-of-glaciology/article/tidal-bending-and-strand-cracks-at-the-kamb-ice-stream-grounding-line-west-antarctica/5A487CC0B853AE66E42D7214EE5CC04A)
 454 [www.cambridge.org/core/journals/journal-of-glaciology/article/tidal-bending](https://www.cambridge.org/core/journals/journal-of-glaciology/article/tidal-bending-and-strand-cracks-at-the-kamb-ice-stream-grounding-line-west-antarctica/5A487CC0B853AE66E42D7214EE5CC04A)
 455 [-and-strand-cracks-at-the-kamb-ice-stream-grounding-line-west-antarctica/](https://www.cambridge.org/core/journals/journal-of-glaciology/article/tidal-bending-and-strand-cracks-at-the-kamb-ice-stream-grounding-line-west-antarctica/5A487CC0B853AE66E42D7214EE5CC04A)
 456 [5A487CC0B853AE66E42D7214EE5CC04A](https://www.cambridge.org/core/journals/journal-of-glaciology/article/tidal-bending-and-strand-cracks-at-the-kamb-ice-stream-grounding-line-west-antarctica/5A487CC0B853AE66E42D7214EE5CC04A) (Publisher: Cambridge University Press) doi:
 457 10.1017/jog.2016.74

458 Huth, A., Adcroft, A., Sergienko, O., & Khan, N. (2022). Ocean currents break up
 459 a tabular iceberg. *Science Advances*, 8(42), eabq6974. Retrieved from [https://www](https://www.science.org/doi/abs/10.1126/sciadv.abq6974)
 460 [.science.org/doi/abs/10.1126/sciadv.abq6974](https://www.science.org/doi/abs/10.1126/sciadv.abq6974) doi: 10.1126/sciadv.abq6974

461 Huth, A., Duddu, R., & Smith, B. (2021). A Generalized Interpolation Material Point
 462 Method for Shallow Ice Shelves. 2: Anisotropic Nonlocal Damage Mechanics and Rift
 463 Propagation. *Journal of Advances in Modeling Earth Systems*, 13(8), e2020MS002292.
 464 Retrieved 2023-04-20, from [https://onlinelibrary.wiley.com/doi/abs/10.1029/](https://onlinelibrary.wiley.com/doi/abs/10.1029/2020MS002292)
 465 [2020MS002292](https://onlinelibrary.wiley.com/doi/abs/10.1029/2020MS002292) (eprint: <https://onlinelibrary.wiley.com/doi/pdf/10.1029/2020MS002292>)
 466 doi: 10.1029/2020MS002292

467 Jeong, S., Howat, I. M., & Bassis, J. N. (2016). Accelerated ice shelf rifting and re-
 468 treat at pine island glacier, west antarctica. *Geophysical Research Letters*, 43(22), 11,720-
 469 11,725. Retrieved from [https://agupubs.onlinelibrary.wiley.com/doi/abs/10.1002/](https://agupubs.onlinelibrary.wiley.com/doi/abs/10.1002/2016GL071360)
 470 [2016GL071360](https://agupubs.onlinelibrary.wiley.com/doi/abs/10.1002/2016GL071360) doi: <https://doi.org/10.1002/2016GL071360>

- 471 Jiménez, S., & Duddu, R. (2018). On the evaluation of the stress intensity factor in
 472 calving models using linear elastic fracture mechanics. *Journal of Glaciology*, *64*(247),
 473 759–770. doi: 10.1017/jog.2018.64
- 474 Jordan, J. R., Holland, P. R., Jenkins, A., Piggott, M. D., & Kimura, S. (2014). Mod-
 475 eling ice-ocean interaction in ice-shelf crevasses. *Journal of Geophysical Research: Oceans*,
 476 *119*(2), 995–1008. Retrieved from [https://agupubs.onlinelibrary.wiley.com/doi/](https://agupubs.onlinelibrary.wiley.com/doi/abs/10.1002/2013JC009208)
 477 [abs/10.1002/2013JC009208](https://agupubs.onlinelibrary.wiley.com/doi/abs/10.1002/2013JC009208) doi: <https://doi.org/10.1002/2013JC009208>
- 478 Joughin, I., Shapero, D., Smith, B., Dutrieux, P., & Barham, M. (2021). Ice-shelf re-
 479 treat drives recent pine island glacier speedup. *Science Advances*, *7*(24), eabg3080. Re-
 480 trieved from <https://www.science.org/doi/abs/10.1126/sciadv.abg3080> doi: 10
 481 .1126/sciadv.abg3080
- 482 Lai, C.-Y., Kingslake, J., Wearing, M. G., Chen, P.-H. C., Gentine, P., Li, H., ... van
 483 Wessem, J. M. (2020). Vulnerability of antarctica’s ice shelves to meltwater-driven frac-
 484 ture. *Nature*, *584*, 574–578. doi: <https://doi.org/10.1038/s41586-020-2627-8>
- 485 Lawn, B. (1993). *Fracture of brittle solids* (2nd ed.). Cambridge University Press.
 486 doi: 10.1017/CBO9780511623127
- 487 Lawrence, J. D., Washam, P. M., Stevens, C., Hulbe, C., Horgan, H. J., Dunbar, G., ...
 488 Schmidt, B. E. (2023, March). Crevasse refreezing and signatures of retreat observed
 489 at Kamb Ice Stream grounding zone. *Nature Geoscience*, *16*(3), 238–243. Retrieved
 490 from <https://doi.org/10.1038/s41561-023-01129-y> doi: 10.1038/s41561-023-01129-
 491 -y
- 492 LeB. Hooke, R. (1981). Flow law for polycrystalline ice in glaciers: Comparison of the-
 493 oretical predictions, laboratory data, and field measurements. *Reviews of Geophysics*,
 494 *19*(4), 664–672. Retrieved from [https://agupubs.onlinelibrary.wiley.com/doi/](https://agupubs.onlinelibrary.wiley.com/doi/abs/10.1029/RG019i004p00664)
 495 [abs/10.1029/RG019i004p00664](https://agupubs.onlinelibrary.wiley.com/doi/abs/10.1029/RG019i004p00664) doi: <https://doi.org/10.1029/RG019i004p00664>
- 496 Lindstrom, D., & MacAyeal, D. (1987). Environmental constraints on west antarctic
 497 ice-sheet formation. *Journal of Glaciology*, *33*(115), 346–356. doi: 10.3189/S0022143000008947
 498
- 499 Lipovsky, B. P. (2020). Ice shelf rift propagation: stability, three-dimensional effects,
 500 and the role of marginal weakening. *The Cryosphere*, *14*(5), 1673–1683. Retrieved from
 501 <https://tc.copernicus.org/articles/14/1673/2020/> doi: 10.5194/tc-14-1673-2020
 502
- 503 Luckman, A., Jansen, D., Kulesa, B., King, E. C., Sammonds, P., & Benn, D. I. (2012).
 504 Basal crevasses in larsen c ice shelf and implications for their global abundance. *The*
 505 *Cryosphere*, *6*, 113–123. doi: 10.5194/tc-6-113-2012
- 506 MacAyeal, D. R. (1989). Large-scale ice flow over a viscous basal sediment: Theory
 507 and application to ice stream b, antarctica. *Journal of Geophysical Research: Solid Earth*,
 508 *94*(B4), 4071–4087. Retrieved from [https://agupubs.onlinelibrary.wiley.com/doi/](https://agupubs.onlinelibrary.wiley.com/doi/abs/10.1029/JB094iB04p04071)
 509 [abs/10.1029/JB094iB04p04071](https://agupubs.onlinelibrary.wiley.com/doi/abs/10.1029/JB094iB04p04071) doi: <https://doi.org/10.1029/JB094iB04p04071>
- 510 Massom, R. A., Scambos, T. A., Bennetts, L. G., Reid, P., Squire, V. A., & Stammer-
 511 john, S. E. (2018, June). Antarctic ice shelf disintegration triggered by sea ice loss and
 512 ocean swell. *Nature*, *558*(7710), 383–389. Retrieved 2023-02-27, from [https://www](https://www.nature.com/articles/s41586-018-0212-1)
 513 [.nature.com/articles/s41586-018-0212-1](https://www.nature.com/articles/s41586-018-0212-1) (Number: 7710 Publisher: Nature Pub-
 514 lishing Group) doi: 10.1038/s41586-018-0212-1
- 515 McGrath, D., Steffen, K., Rajaram, H., Scambos, T., Abdalati, W., & Rignot, E. (2012).
 516 Basal crevasses on the larsen c ice shelf, antarctica: Implications for meltwater ponding

- 517 and hydrofracture. *Geophysical Research Letters*, 39(16). Retrieved from [https://](https://agupubs.onlinelibrary.wiley.com/doi/abs/10.1029/2012GL052413)
 518 [agupubs.onlinelibrary.wiley.com/doi/abs/10.1029/2012GL052413](https://doi.org/10.1029/2012GL052413) doi: [https://](https://doi.org/10.1029/2012GL052413)
 519 doi.org/10.1029/2012GL052413
- 520 McGrath, D., Steffen, K., Scambos, T., Rajaram, H., Casassa, G., & Rodriguez Lagos,
 521 J. L. (2012). Basal crevasses and associated surface crevassing on the larsen c ice shelf,
 522 antarctica, and their role in ice-shelf instability. *Annals of Glaciology*, 53(60), 10–18.
 523 doi: 10.3189/2012AoG60A005
- 524 Morris, E. M., & Vaughan, D. G. (2003). Spatial and temporal variation of surface
 525 temperature on the antarctic peninsula and the limit of viability of ice shelves. *Antarc-*
 526 *tic Research Series*, 79(10.1029).
- 527 Mouginot, J., Scheuchl, B., & Rignot, E. (2017). *Measures antarctic boundaries for*
 528 *ipy 2007-2009 from satellite radar, version 2*. (Boulder, Colorado USA. NASA National
 529 Snow and Ice Data Center Distributed Active Archive Center. doi: [http://dx.doi.org/](http://dx.doi.org/10.5067/AXE4121732AD)
 530 [10.5067/AXE4121732AD](http://dx.doi.org/10.5067/AXE4121732AD). Accessed 10/07/2023.)
- 531 Murray, T., Selmes, N., James, T. D., Edwards, S., Martin, I., O'Farrell, T., ... Baugé,
 532 T. (2015). Dynamics of glacier calving at the ungrounded margin of helheim glacier,
 533 southeast greenland. *Journal of Geophysical Research: Earth Surface*, 120(6), 964-982.
 534 Retrieved from <https://agupubs.onlinelibrary.wiley.com/doi/abs/10.1002/2015JF003531>
 535 doi: <https://doi.org/10.1002/2015JF003531>
- 536 Nick, F., Van Der Veen, C., Vieli, A., & Benn, D. (2010). A physically based calving
 537 model applied to marine outlet glaciers and implications for the glacier dynamics. *Jour-*
 538 *nal of Glaciology*, 56(199), 781–794. doi: 10.3189/002214310794457344
- 539 Nye, J. F. (1955). Comments on dr. loewe's letter and notes on crevasses. *Journal*
 540 *of Glaciology*, 2(17), 512–514. doi: 10.3189/S0022143000032652
- 541 Pralong, A., & Funk, M. (2005). Dynamic damage model of crevasse opening and ap-
 542 plication to glacier calving. *Journal of Geophysical Research: Solid Earth*, 110(B1). Re-
 543 trieved from <https://agupubs.onlinelibrary.wiley.com/doi/abs/10.1029/2004JB003104>
 544 doi: <https://doi.org/10.1029/2004JB003104>
- 545 Pritchard, H., Ligtenberg, S., Fricker, H., Vaughan, D., van den Broeke, M., & Padman,
 546 L. (2012). Antarctic ice loss driven by ice-shelf melt. *Nature*, 484, 502–505.
- 547 Ranganathan, M., Minchew, B., Meyer, C. R., & Peč, M. (2021). Recrystallization of
 548 ice enhances the creep and vulnerability to fracture of ice shelves. *Earth and Planetary*
 549 *Science Letters*, 576, 117219. Retrieved from [https://www.sciencedirect.com/science/](https://www.sciencedirect.com/science/article/pii/S0012821X2100474X)
 550 [article/pii/S0012821X2100474X](https://www.sciencedirect.com/science/article/pii/S0012821X2100474X) doi: <https://doi.org/10.1016/j.epsl.2021.117219>
- 551 Reeh, N. (1968). On the calving of ice from floating glaciers and ice shelves. *Journal*
 552 *of Glaciology*, 7(50), 215–232. doi: 10.3189/S0022143000031014
- 553 Rignot, E., Casassa, G., Gogineni, P., Krabill, W., Rivera, A., & Thomas, R. (2004).
 554 Accelerated ice discharge from the antarctic peninsula following the collapse of larsen
 555 b ice shelf. *Geophysical Research Letters*, 31(18). Retrieved from [https://agupubs](https://agupubs.onlinelibrary.wiley.com/doi/abs/10.1029/2004GL020697)
 556 [.onlinelibrary.wiley.com/doi/abs/10.1029/2004GL020697](https://agupubs.onlinelibrary.wiley.com/doi/abs/10.1029/2004GL020697) doi: [https://doi.org/](https://doi.org/10.1029/2004GL020697)
 557 [10.1029/2004GL020697](https://doi.org/10.1029/2004GL020697)
- 558 Rist, M. A., Sammonds, P. R., Oerter, H., & Doake, C. S. M. (2002). Fracture of antarctic
 559 shelf ice. *Journal of Geophysical Research: Solid Earth*, 107(B1), ECV 2-1-ECV 2-
 560 13. Retrieved from [https://agupubs.onlinelibrary.wiley.com/doi/abs/10.1029/](https://agupubs.onlinelibrary.wiley.com/doi/abs/10.1029/2000JB000058)
 561 [2000JB000058](https://agupubs.onlinelibrary.wiley.com/doi/abs/10.1029/2000JB000058) doi: <https://doi.org/10.1029/2000JB000058>

- 562 Robin, G. d. Q. (1955). Ice movement and temperature distribution in glaciers and
563 ice sheets. *Journal of Glaciology*, 2(18), 523–532. doi: 10.3189/002214355793702028
564
- 565 Rott, H., Rack, W., Skvarca, P., & Angelis, H. D. (2002). Northern larsen ice shelf,
566 antarctica: further retreat after collapse. *Annals of Glaciology*, 34, 277–282. doi: 10
567 .3189/172756402781817716
- 568 Scambos, T., Haran, T., Fahnestock, M., Painter, T., & Bohlander, J. (2007). Modis-
569 based mosaic of antarctica (moa) data sets: Continent-wide surface morphology and snow
570 grain size. *Remote Sensing of Environment*, 111(2), 242–257. Retrieved from [https://](https://www.sciencedirect.com/science/article/pii/S0034425707002854)
571 www.sciencedirect.com/science/article/pii/S0034425707002854 (Remote Sens-
572 ing of the Cryosphere Special Issue) doi: <https://doi.org/10.1016/j.rse.2006.12.020>
- 573 Sergienko, O. V. (2010). Elastic response of floating glacier ice to impact of long-period
574 ocean waves. *Journal of Geophysical Research: Earth Surface*, 115(F4). Retrieved 2023-
575 01-24, from <https://onlinelibrary.wiley.com/doi/abs/10.1029/2010JF001721> (eprint:
576 <https://onlinelibrary.wiley.com/doi/pdf/10.1029/2010JF001721>) doi: 10.1029/2010JF001721
577
- 578 Sergienko, O. V. (2013). Normal modes of a coupled ice-shelf/sub-ice-shelf cavity sys-
579 tem. *Journal of Glaciology*, 59(213), 76–80. Retrieved 2023-02-27, from [https://www](https://www.cambridge.org/core/product/identifier/S0022143000203420/type/journal_article)
580 [.cambridge.org/core/product/identifier/S0022143000203420/type/journal_article](https://www.cambridge.org/core/product/identifier/S0022143000203420/type/journal_article)
581 doi: 10.3189/2013JoG12J096
- 582 Tada, H., Paris, P. C., & Irwin, G. R. (2000). *The Stress Analysis of Cracks Hand-*
583 *book, Third Edition*. ASME Press. Retrieved from <https://doi.org/10.1115/1.801535>
584 doi: 10.1115/1.801535
- 585 Thomas, R. H., & MacAyeal, D. R. (1982). Derived characteristics of the ross ice shelf,
586 antarctica. *Journal of Glaciology*, 28(100), 397–412. doi: 10.3189/S0022143000005025
587
- 588 van der Veen, C. (1998). Fracture mechanics approach to penetration of bottom crevasses
589 on glaciers. *Cold Regions Science and Technology*, 27(3), 213–223. doi: [https://doi](https://doi.org/10.1016/S0165-232X(98)00006-8)
590 [.org/10.1016/S0165-232X\(98\)00006-8](https://doi.org/10.1016/S0165-232X(98)00006-8)
- 591 van der Veen, C. J. (1999). Crevasses on glaciers. *Polar Geography*, 23(3), 213–245.
592 Retrieved from <https://doi.org/10.1080/10889379909377677> doi: 10.1080/10889379909377677
593
- 594 van Wessem, J. M., van de Berg, W. J., Noël, B. P. Y., van Meijgaard, E., Amory, C.,
595 Birnbaum, G., . . . van den Broeke, M. R. (2018). Modelling the climate and surface
596 mass balance of polar ice sheets using racmo2 – part 2: Antarctica (1979–2016). *The*
597 *Cryosphere*, 12(4), 1479–1498. Retrieved from [https://tc.copernicus.org/articles/](https://tc.copernicus.org/articles/12/1479/2018/)
598 [12/1479/2018/](https://tc.copernicus.org/articles/12/1479/2018/) doi: 10.5194/tc-12-1479-2018
- 599 van Wessem, J. M., van den Broeke, M. R., Wouters, B., & Lhermitte, S. (2023). Vari-
600 able temperature thresholds of melt pond formation on antarctic ice shelves. *Nature*
601 *Climate Change*, 13(2), 161–166.
- 602 Vaughan, D. G. (1995). Tidal flexure at ice shelf margins. *Journal of Geophysical*
603 *Research: Solid Earth*, 100(B4), 6213–6224. Retrieved from [https://agupubs.onlinelibrary](https://agupubs.onlinelibrary.wiley.com/doi/abs/10.1029/94JB02467)
604 [.wiley.com/doi/abs/10.1029/94JB02467](https://agupubs.onlinelibrary.wiley.com/doi/abs/10.1029/94JB02467) doi: <https://doi.org/10.1029/94JB02467>
605
- 606 Wagner, T. J. W., James, T. D., Murray, T., & Vella, D. (2016). On the role of buoy-
607 ant flexure in glacier calving. *Geophysical Research Letters*, 43(1), 232–240A. Retrieved

- 608 from <https://agupubs.onlinelibrary.wiley.com/doi/abs/10.1002/2015GL067247>
609 doi: <https://doi.org/10.1002/2015GL067247>
- 610 Wagner, T. J. W., Wadhams, P., Bates, R., Elosegui, P., Stern, A., Vella, D., ... Nicholls,
611 K. W. (2014). The “footloose” mechanism: Iceberg decay from hydrostatic stresses.
612 *Geophysical Research Letters*, *41*(15), 5522–5529. Retrieved from <https://agupubs.onlinelibrary>
613 [.wiley.com/doi/abs/10.1002/2014GL060832](https://doi.org/10.1002/2014GL060832) doi: <https://doi.org/10.1002/2014GL060832>
614
- 615 Walker, C. C., Bassis, J. N., Fricker, H. A., & Czerwinski, R. J. (2013). Structural and
616 environmental controls on antarctic ice shelf rift propagation inferred from satellite mon-
617 itoring. *Journal of Geophysical Research: Earth Surface*, *118*(4), 2354–2364. Retrieved
618 from <https://agupubs.onlinelibrary.wiley.com/doi/abs/10.1002/2013JF002742>
619 doi: <https://doi.org/10.1002/2013JF002742>
- 620 Wearing, M. G. (2017). The flow dynamics and buttressing of ice shelves phd thesis.
621
- 622 Weertman, J. (1957). Deformation of floating ice shelves. *Journal of Glaciology*, *3*(21),
623 38–42. doi: 10.3189/S0022143000024710
- 624 Weertman, J. (1973). Can a water-filled crevasse reach the bottom surface of a glacier.
625 *IAASH publ*, *95*, 139–145.
- 626 Weertman, J. (1974). Depth of water-filled crevasses that are closely spaced. *Jour-*
627 *nal of Glaciology*, *13*(69), 544–544. doi: 10.3189/S0022143000023297
- 628 Weertman, J. (1977). Penetration depth of closely spaced water-free crevasses. *Jour-*
629 *nal of Glaciology*, *18*(78), 37–46. doi: 10.3189/S0022143000021493
- 630 Wuite, J., Hetzenecker, M., Nagler, T., & Scheiblauer, S. (2021). *Esa antarctic ice sheet*
631 *climate change initiative (antarctic_ice_sheet_cci): Antarctic ice sheet monthly velocity*
632 *from 2017 to 2020, derived from sentinel-1, v1*. NERC EDS Centre for Environmen-
633 tal Data Analysis. Retrieved from <https://dx.doi.org/10.5285/00fe090efc58446e8980992a617f632f>
634 doi: 10.5285/00fe090efc58446e8980992a617f632f
- 635 Zarrinderakht, M., Schoof, C., & Peirce, A. (2022). The effect of hydrology and crevasse
636 wall contact on calving. *The Cryosphere*, *16*(10), 4491–4512. Retrieved from [https://](https://tc.copernicus.org/articles/16/4491/2022/)
637 tc.copernicus.org/articles/16/4491/2022/ doi: 10.5194/tc-16-4491-2022

638 **References from Supporting Information**

- 639 Buck, W. R. (2023). The role of fresh water in driving ice shelf crevassing, rifting
640 and calving. *Earth and Planetary Science Letters*, *624*, 118444. Retrieved from
641 <https://www.sciencedirect.com/science/article/pii/S0012821X23004570> doi:
642 <https://doi.org/10.1016/j.epsl.2023.118444>
- 643 Chartrand, R. (2017). Numerical differentiation of noisy, nonsmooth, multidimen-
644 sional data. In *2017 IEEE Global Conference on Signal and Information Processing*
645 *(globalsip)* (p. 244–248). doi: 10.1109/GlobalSIP.2017.8308641
- 646 Craven, M., Allison, I., Fricker, H. A., Warner, R. (2009). Properties of a marine
647 ice layer under the amery ice shelf, east antarctica. *Journal of Glaciology*, *55*(192),
648 717–728. doi: 10.3189/002214309789470941
- 649 Fowler, A., Ng, F. (2020). *Glaciers and ice sheets in the climate system: The*
650 *karthaus summer school lecture notes*. Springer Nature.

- 651 Hulbe, C. L., Rignot, E., Macayeal, D. R. (1998). Comparison of ice-shelf creep flow
652 simulations with ice-front motion of filchner-ronne ice shelf, antarctica, detected by
653 sar interferometry. *Annals of Glaciology*, 27, 182–186. doi: 10.3189/1998AoG27-1
654 -182-186
- 655 Jeong, S., Howat, I. M., Bassis, J. N. (2016). Accelerated ice shelf rifting and re-
656 treat at pine island glacier, west antarctica. *Geophysical Research Letters*, 43(22),
657 11,720–11,725. Retrieved from [https://agupubs.onlinelibrary.wiley.com/doi/
658 abs/10.1002/2016GL071360](https://agupubs.onlinelibrary.wiley.com/doi/abs/10.1002/2016GL071360) doi: <https://doi.org/10.1002/2016GL071360>
- 659 Jezek, K. C. (1984). A modified theory of bottom crevasses used as a means
660 for measuring the buttressing effect of ice shelves on inland ice sheets. *Jour-
661 nal of Geophysical Research: Solid Earth*, 89(B3), 1925–1931. Retrieved from
662 <https://agupubs.onlinelibrary.wiley.com/doi/abs/10.1029/JB089iB03p01925>
663 doi: <https://doi.org/10.1029/JB089iB03p01925>
- 664 LeB. Hooke, R. (1981). Flow law for polycrystalline ice in glaciers: Com-
665 parison of theoretical predictions, laboratory data, and field measurements.
666 *Reviews of Geophysics*, 19(4), 664–672. Retrieved from [https://agupubs
667 .onlinelibrary.wiley.com/doi/abs/10.1029/RG019i004p00664](https://agupubs.onlinelibrary.wiley.com/doi/abs/10.1029/RG019i004p00664) doi:
668 <https://doi.org/10.1029/RG019i004p00664>
- 669 MacAyeal, D. R. (1989). Large-scale ice flow over a viscous basal sediment: The-
670 ory and application to ice stream b, antarctica. *Journal of Geophysical Research:
671 Solid Earth*, 94(B4), 4071–4087. Retrieved from [https://agupubs.onlinelibrary
672 .wiley.com/doi/abs/10.1029/JB094iB04p04071](https://agupubs.onlinelibrary.wiley.com/doi/abs/10.1029/JB094iB04p04071) doi: [https://doi.org/10.1029/
JB094iB04p04071](https://doi.org/10.1029/
673 JB094iB04p04071)
- 674 MacAyeal, D. R., Rignot, E., Hulbe, C. L. (1998). Ice-shelf dynamics near the
675 front of the filchner-ronne ice shelf, antarctica, revealed by sar interferometry:
676 model/interferogram comparison. *Journal of Glaciology*, 44(147), 419–428. doi:
677 10.3189/S0022143000002744
- 678 Morlighem, M. (2020). *Measures bedmachine antarctica, version 2*. NASA Na-
679 tional Snow and Ice Data Center Distributed Active Archive Center. Retrieved from
680 <https://nsidc.org/data/NSIDC-0756/versions/2> doi: 10.5067/E1QL9HFQ7A8M
- 681 Morlighem, M., Rignot, E., Binder, T., Blankenship, D., Drews, R., Eagles, G., .
682 . . others (2020). Deep glacial troughs and stabilizing ridges unveiled beneath the
683 margins of the antarctic ice sheet. *Nature Geoscience*, 13(2), 132–137.
- 684 Mouginot, J., Rignot, E., Scheuchl, B., Millan, R. (2017). Comprehensive annual
685 ice sheet velocity mapping using landsat-8, sentinel-1, and radarsat-2 data. *Remote
686 Sensing*, 9(4). Retrieved from <https://www.mdpi.com/2072-4292/9/4/364> doi:
687 10.3390/rs9040364
- 688 Mouginot, J., Scheuchl, B., Rignot, E. (2012). Mapping of ice motion in antarctica
689 using synthetic-aperture radar data. *Remote Sensing*, 4(9), 2753–2767. Retrieved
690 from <https://www.mdpi.com/2072-4292/4/9/2753> doi: 10.3390/rs4092753
- 691 Nicholls, K. W., Corr, H. F., Stewart, C. L., Lok, L. B., Brennan, P. V., Vaughan,
692 D. G. (2015). A ground-based radar for measuring vertical strain rates and time-
693 varying basal melt rates in ice sheets and shelves. *Journal of Glaciology*, 61(230),
694 1079–1087. doi: 10.3189/2015JoG15J073
- 695 Nye, J. F. (1955). Comments on dr. loewe’s letter and notes on crevasses. *Journal of
696 Glaciology*, 2(17), 512–514. doi: 10.3189/S0022143000032652

- 697 Reeh, N. (1968). On the calving of ice from floating glaciers and ice shelves. *Journal*
698 *of Glaciology*, 7(50), 215–232. doi: 10.3189/S0022143000031014
- 699 Rignot, E., MacAyeal, D. R. (1998). Ice-shelf dynamics near the front of the filch-
700 ner—ronne ice shelf, antarctica, revealed by sar interferometry. *Journal of Glaciol-*
701 *ogy*, 44(147), 405–418. doi: 10.3189/S0022143000002732
- 702 Rignot, E., Mouginot, J., Scheuchl, B. (2011). Ice flow of the antarctic ice sheet.
703 *Science*, 333(6048), 1427–1430. Retrieved from [https://www.science.org/doi/](https://www.science.org/doi/abs/10.1126/science.1208336)
704 [abs/10.1126/science.1208336](https://www.science.org/doi/abs/10.1126/science.1208336) doi: 10.1126/science.1208336
- 705 Rignot, E., Mouginot, J., Scheuchl, B. (2017). Measures insar-based antarctica ice
706 velocity map, version 2. NASA National Snow and Ice Data Center Distributed
707 Active Archive Center. Retrieved from [https://nsidc.org/data/NSIDC-484/](https://nsidc.org/data/NSIDC-484/versions/2)
708 [versions/2](https://nsidc.org/data/NSIDC-484/versions/2) doi: 10.5067/D7GK8F5J8M8R
- 709 Rist, M. A., Sammonds, P. R., Oerter, H., Doake, C. S. M. (2002). Fracture of
710 antarctic shelf ice. *Journal of Geophysical Research: Solid Earth*, 107(B1), ECV
711 2-1-ECV 2-13. Retrieved from [https://agupubs.onlinelibrary.wiley.com/doi/](https://agupubs.onlinelibrary.wiley.com/doi/abs/10.1029/2000JB000058)
712 [abs/10.1029/2000JB000058](https://agupubs.onlinelibrary.wiley.com/doi/abs/10.1029/2000JB000058) doi: <https://doi.org/10.1029/2000JB000058>
- 713 Robin, G. d. Q. (1955). Ice movement and temperature distribution in glaciers and
714 ice sheets. *Journal of Glaciology*, 2(18), 523–532. doi: 10.3189/002214355793702028
- 715 Sandhäger, H., Rack, W., Jansen, D. (2005). Model investigations of larsen b ice
716 shelf dynamics prior to the breakup. *FRISP Rep*, 16, 5–12.
- 717 Sergienko, O. V. (2014). A vertically integrated treatment of ice stream and ice shelf
718 thermodynamics. *Journal of Geophysical Research: Earth Surface*, 119(4), 745–757.
719 Retrieved from [https://agupubs.onlinelibrary.wiley.com/doi/abs/10.1002/](https://agupubs.onlinelibrary.wiley.com/doi/abs/10.1002/2013JF002908)
720 [2013JF002908](https://agupubs.onlinelibrary.wiley.com/doi/abs/10.1002/2013JF002908) doi: <https://doi.org/10.1002/2013JF002908>
- 721 Sergienko, O. V., Goldberg, D. N., Little, C. M. (2013). Alternative ice shelf equi-
722 libria determined by ocean environment. *Journal of Geophysical Research: Earth*
723 *Surface*, 118(2), 970–981. Retrieved from [https://agupubs.onlinelibrary.wiley](https://agupubs.onlinelibrary.wiley.com/doi/abs/10.1002/jgrf.20054)
724 [.com/doi/abs/10.1002/jgrf.20054](https://agupubs.onlinelibrary.wiley.com/doi/abs/10.1002/jgrf.20054) doi: <https://doi.org/10.1002/jgrf.20054>
- 725 Taylor, J. R. (1982). *An introduction to error analysis: the study of uncertainties in*
726 *physical measurements* (Vol. 2). Springer.
- 727 Thomas, R. H., MacAyeal, D. R. (1982). Derived characteristics of the ross
728 ice shelf, antarctica. *Journal of Glaciology*, 28(100), 397–412. doi: 10.3189/
729 S0022143000005025
- 730 Tyler, S., Holland, D., Zagorodnov, V., Stern, A., Sladek, C., Kobs, S., . . . Bryen-
731 ton, J. (2013). Using distributed temperature sensors to monitor an antarctic ice
732 shelf and sub-ice-shelf cavity. *Journal of Glaciology*, 59(215), 583–591. doi: 10.3189/
733 2013JoG12J207
- 734 van den Broeke, M. (2008). Depth and density of the antarctic firn layer. *Arctic,*
735 *Antarctic, and Alpine Research*, 40(2), 432–438.
- 736 van Wessem, J. M., van de Berg, W. J., Noël, B. P. Y., van Meijgaard, E., Amory,
737 C., Birnbaum, G., . . . van den Broeke, M. R. (2018). Modelling the climate
738 and surface mass balance of polar ice sheets using racmo2 – part 2: Antarc-
739 tica (1979–2016). *The Cryosphere*, 12(4), 1479–1498. Retrieved from [https://](https://tc.copernicus.org/articles/12/1479/2018/)
740 tc.copernicus.org/articles/12/1479/2018/ doi: 10.5194/tc-12-1479-2018
- 741 Wagner, T. J. W., James, T. D., Murray, T., Vella, D. (2016). On the role of buoy-
742 ant flexure in glacier calving. *Geophysical Research Letters*, 43(1), 232–240A. Re-

- 743 retrieved from <https://agupubs.onlinelibrary.wiley.com/doi/abs/10.1002/>
744 2015GL067247 doi: <https://doi.org/10.1002/2015GL067247>
- 745 Walker, C. C., Bassis, J. N., Fricker, H. A., Czerwinski, R. J. (2013). Structural and
746 environmental controls on antarctic ice shelf rift propagation inferred from satellite
747 monitoring. *Journal of Geophysical Research: Earth Surface*, 118(4), 2354-2364.
748 Retrieved from <https://agupubs.onlinelibrary.wiley.com/doi/abs/10.1002/>
749 2013JF002742 doi: <https://doi.org/10.1002/2013JF002742>
- 750 Wearing, M. G. (2017). The flow dynamics and buttressing of ice shelves phd thesis.
- 751 Weertman, J. (1957). Deformation of floating ice shelves. *Journal of Glaciology*,
752 3(21), 38–42. doi: 10.3189/S0022143000024710
- 753 Wuite, J., Hetzenecker, M., Nagler, T., Scheiblauer, S. (2021). *Esa antarctic*
754 *ice sheet climate change initiative (antarctic ice sheet cci): Antarctic*
755 *ice sheet monthly velocity from 2017 to 2020, derived from sentinel-1,*
756 *v1*. NERC EDS Centre for Environmental Data Analysis. Retrieved from
757 <https://dx.doi.org/10.5285/00fe090efc58446e8980992a617f632f> doi: 10
758 .5285/00fe090efc58446e8980992a617f632f
- 759 Zarrinderakht, M., Schoof, C., Peirce, A. (2022). The effect of hydrology and
760 crevasse wall contact on calving. *The Cryosphere*, 16(10), 4491–4512. Retrieved
761 from <https://tc.copernicus.org/articles/16/4491/2022/> doi: 10.5194/tc-16
762 -4491-2022

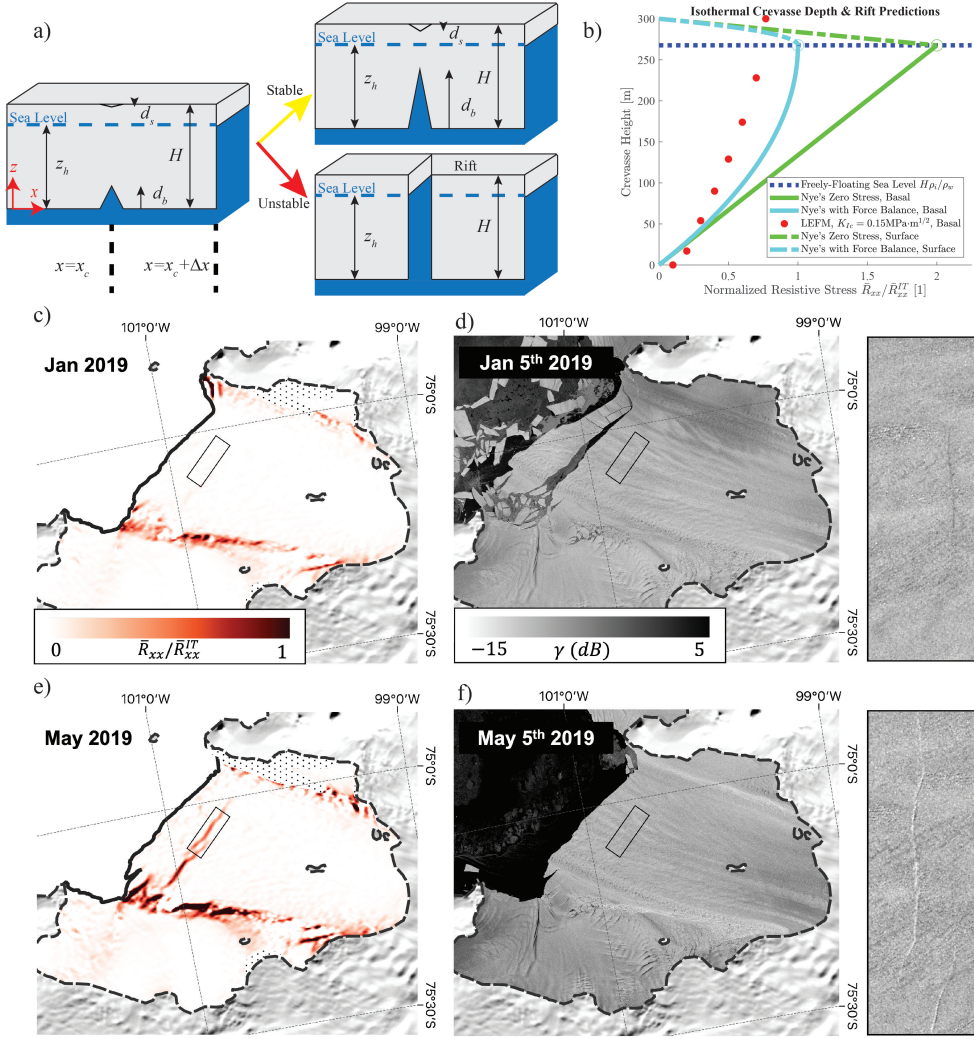


Figure 1. a) Schematic of crevasse propagating stably or unstably and forming a full-thickness fracture called a rift. Crevasse depths d_s , d_b , thickness H , coordinate system, and piezometric head at sea level z_h are illustrated. b) Several previously existing isothermal crevasse depth predictions versus depth-averaged resistive stress \bar{R}_{xx} normalized by the analytical depth-averaged resistive stress \bar{R}_{xx}^{IT} for an unconfined ice tongue with $H=300$ meters. Circular red dots are LEFM basal crevasse depth numerical predictions, solid lines are basal crevasse depth analytical theory, and dash-dotted lines are surface crevasse depth analytical theory. Rifts initiate either where $d_b=H$ for LEFM or at the open circles that denote the intersection of surface and basal crevasse tips for Nye’s Zero-Stress approximation. Formulations based on Nye’s theory require surface and basal crevasse for theoretical consistency, whereas LEFM treats an isolated basal crevasse. Subfigures c) to f) show a potential instance of the basal crevasse-to-rift transition (Jeong et al., 2016; Joughin et al., 2021) over Pine Island Ice Shelf during January to May 2019. c) An estimate of the ratio $\bar{R}_{xx}/\bar{R}_{xx}^{IT}$ over Pine Island Ice Shelf in January 2019, found using ice velocity data averaged over the month of January 2019 (Wuite et al., 2021). d) SAR backscatter image at 50m resolution from 5th January 2019, and a close-up showing the terminus region of Pine Island Ice Shelf where a fracture (can be surface crack, surface expression of basal crack or rift) is dimly visible. e) The equivalent of (c) for May 2019. f) A backscatter image from May 2019 where a rift is clearly visible. Grounding lines according to Mouginot et al. (2017) are shown with a dashed black line. Grounded ice is masked with a MODIS Mosaic of Antarctica (Haran et al., 2013). Calving fronts are marked with a black line.

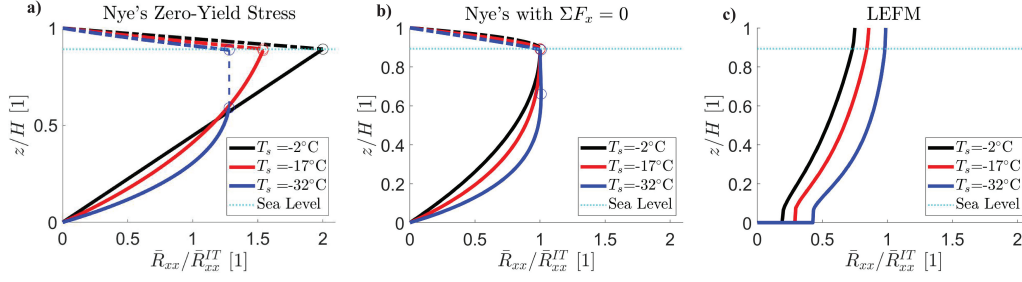


Figure 2. Predicted crevasse depths for a) Nye's theory, b) Nye's with horizontal force balance, and c) linear elastic fracture mechanics given a linear temperature profile in the vertical direction from a basal temperature of -2°C to surface temperature T_s . The y-axes are nondimensional height from the ice shelf base, and the x-axes are depth-averaged resistive stress normalized by depth-averaged ice tongue resistive stress. The solid lines are the basal crack depths, the dash-dotted lines are surface crevasse depths, and the vertical dashed lines and circles are where unstable basal crevasses propagate to meet surface crevasses for the given B and linear $T(z)$. The isothermal cases presented here at $T = -2^\circ\text{C}$ of Nye's and Nye's with Horizontal Force Balance are analytical, while all other results are numerical.

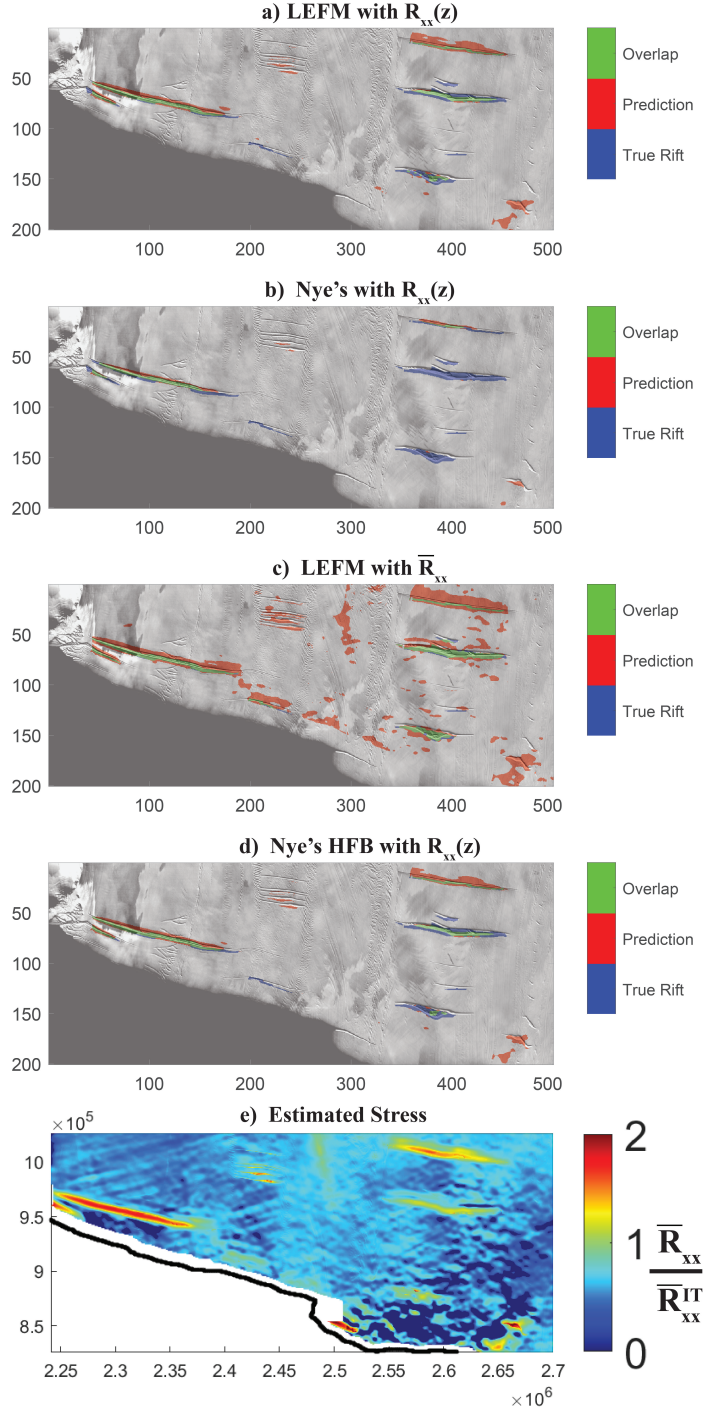


Figure 3. a) to d) are map views in kilometers of observed ((Walker et al., 2013); labeled as true rifts in blue) and theoretically predicted rifts (red) on the Ross Ice Shelf, overlain on MODIS MOA 2014 (Haran et al., 2018; Scambos et al., 2007), with correctly predicted rifts in green. Rift formation theories are a) LEFM with depth-varying stress due to temperature variation $R_{xx}(z)$, b) Nye's with $R_{xx}(z)$, c) LEFM with depth-averaged stress \bar{R}_{xx} , and d) Nye's with Horizontal Force Balance with $R_{xx}(z)$. e) is the estimated stress used for panel (a-d), with axes in meters. Known rifts are padded with locally unbroken ice thickness.

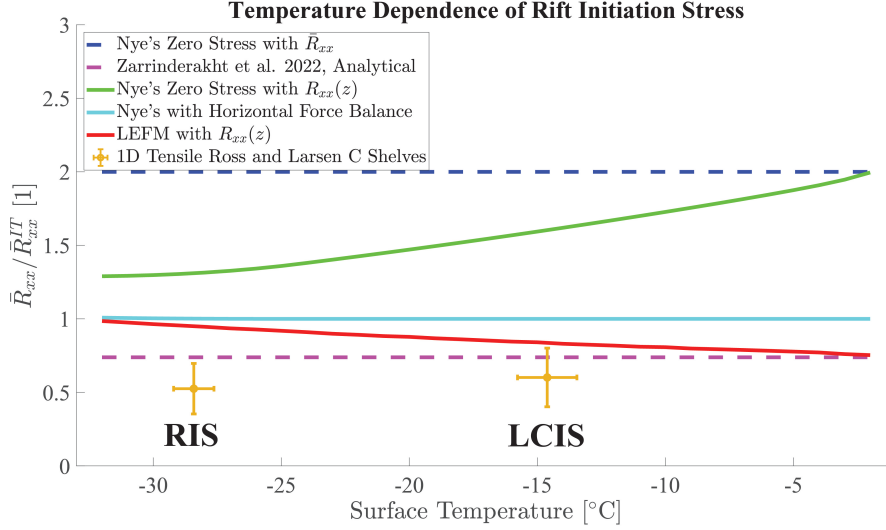


Figure 4. Nondimensional resistive stress required to initiate rifts versus surface temperature. The solid lines account for vertically-varying temperature structure through depth-varying stress $R_{xx}(z)$, whereas the dashed lines utilize depth-averaged resistive stress \bar{R}_{xx} . For a given theory, the region above and below the curve are predicted as a rift and non-rift, respectively. Extensional ice shelf data that is not rifted and upholds the 1D fracture assumptions is plotted in orange with mean and standard deviation. This data is shown in map view in Figure S4. We use the average thickness in the unbroken area surrounding the rifts as H to calculate \bar{R}_{xx}^{IT} . In this figure, surface temperatures colder than -25°C are on the Ross Ice Shelf (RIS), whereas those warmer are on the Larsen C Ice Shelf (LCIS). While the (Zarrinderakht et al., 2022) line in dashed magenta looks compelling with the intact ice shelf data in orange, map view analyses (see Figures 3c), S3c)) show that it overpredicts rifts.